Applied Physics Letters ARTICLE pubs.aip.org/aip/apl

Double-barrier magnetic tunnel junctions with enhanced tunnel magnetoresistance

Cite as: Appl. Phys. Lett. **125**, 223503 (2024); doi: 10.1063/5.0235559
Submitted: 28 August 2024 · Accepted: 13 November 2024 ·
Published Online: 25 November 2024

Xiaohong Zheng,[1,a)] Shili Yang,[1] Zhifan Zheng,[1] Chun-Sheng Liu,[2] Weiyang Wang,[3,a)] and Lei Zhang[4,5]

AFFILIATIONS

[1]College of Information Science and Technology, Nanjing Forestry University, Nanjing 210037, China
[2]College of Electronic and Optical Engineering, Nanjing University of Posts and Telecommunications, Nanjing 210023, China
[3]Shangrao Open University, Shangrao, Jiangxi 334001, China
[4]State Key Laboratory of Quantum Optics and Quantum Optics Devices, Institute of Laser Spectroscopy, Shanxi University, Taiyuan 030006, China
[5]Collaborative Innovation Center of Extreme Optics, Shanxi University, Taiyuan 030006, China

[a)]**Authors to whom correspondence should be addressed:** xhzheng@njfu.edu.cn and wywang_theory@foxmail.com

ABSTRACT

Tunnel magnetoresistance (TMR) ratio is a key parameter characterizing the performance of a magnetic tunnel junction (MTJ), and a large TMR ratio is essential for the practical application of it. Generally, the traditional solutions to increasing the TMR ratio are to choose different material combinations as the ferromagnetic (FM) leads and nonmagnetic tunnel barrier. In this work, we study an architecture of MTJs of "FM/barrier/FM/barrier/FM" with double barriers, in contrast to the traditional single barrier structure "FM/barrier/FM." We first analytically show that double barrier MTJ will generally have much higher TMR ratio than the single barrier MTJ and then substantiate it with the well-known example of "Fe/MgO/Fe" MTJ. Based on density functional calculations combined with nonequilibrium Green's function technique for quantum transport study, in the single barrier "Fe/MgO/Fe" MTJ, the TMR ratio is obtained as 122%, while in the double barrier "Fe/MgO/Fe/MgO/Fe" MTJ, it is greatly increased to 802%, suggesting that double barrier design can greatly enhance the TMR and can be taken into consideration in the design of MTJs.

Since the discovery of giant magnetoresistance effect in magnetic tunnel junctions (MTJs) by Baibich *et al.*[1] and Binasch *et al.*,[2] spin of electrons as a carrier of information started to attract intensive attention,[3–9] and the data storage technique based on it greatly decreases the energy consumption and greatly increases the storage density.[10–13] The basic principle of MTJs is the electron tunneling, which is a quantum mechanical effect, usually demonstrated in a trilayer system consisting of two metallic electrodes separated by a thin insulator. More fundamentally, the tunneling probability originates from the complex band structure[14–16] of the insulator. In general material simulation, we diagonalize the Hamiltonian matrix for each k wave vector and get a set of eigen values that are all real $[E = H(k)]$. Each (E, k) pair means a propagating Bloch state. However, for transport study, since we are dealing with a problem of how an electron with certain energy E will propagate across a crystal, we often solve the inverse problem $[k = H(E)]$ by diagonalizing the Hamiltonian matrix for a certain E to get k. We will also get a set of k values, but some are real, and the others are complex, namely, $k = k_1 + ik_2$. The real k is still a Bloch state component that propagates through the whole crystal, while the complex k means a wave function with a factor $e^{ikx} = e^{ik_1x - k_2x}$, where e^{-k_2x} is an exponentially decaying factor, meaning that it can only exist for a very short distance. Thus, such decaying modes are not observable in the interior of the crystal but exist near the edge of the crystal and actually act as the transport channels for electrons that come across the interface from another material. Due to the exponential decaying feature, the electron transmission probability will decrease exponentially with the propagating distance.

In MTJs, the two electrodes are ferromagnets, such as Fe or Co, with one electrode relatively hard and one relatively soft and easy to flip its magnetization direction.[17–19] In magnetic systems, the electron scattering is spin dependent. Thus, when the magnetization in the soft magnetic electrode is reversed, the transmission of both spin channels will be affected and, accordingly, the total transmission $T(E)$ will be changed, which leads to the tunnel magnetoresistance.[20,21] A giant tunnel magnetoresistance (TMR) ratio is crucial for practical applications of MTJs; thus, numerous significant theoretical and experimental

efforts have been taken to create MTJs with different ferromagnetic metals and insulating materials in order to generate large TMR ratios. MgO and Al_2O_3 are the most commonly used barrier materials in traditional MTJs,[22–25] and particularly MgO MTJs with large TMRs are greatly useful in many fields, such as field sensing and nonvolatile magnetic random access memories. As such, much attention has been paid to increase the TMR ratio of the MgO barrier based MTJs. For example, at room temperature, TMR of configurations like Fe/MgO/Fe, Co/MgO/Co, and CoFeB/MgO/CoFeB have been reported to be 180%, 401%, and 603%, respectively.[25–27] Recently, 5000% TMR ratio has been achieved in FeAl/MgO/FeAl MTJ.[28] Obviously, choices of different electrodes can lead to greatly enhanced TMR ratio.

In this Letter, we intend to report a completely different mechanism that may systematically increase the TMR ratio of MTJs by designing a double barrier (DB), as compared with the single barrier (SB) MTJ. A DB-MTJ is composed of two tunnel barrier in series. Since the pioneering work of Chang *et al.*,[29] much research attention has been paid to the study of such structures. Especially, the current–voltage characteristics of these structures demonstrate useful features at room temperature and high bias, unlike most other mesoscopic phenomena that are limited to low temperature and linear response regime.[30] Recently, the double barrier structure has been utilized to design electronic devices and achieve good performance in them.[31–35] As will be discussed later in this work, DB-MTJ may have higher TMR than the SB-MTJ. This is proved by the pedagogical example of Fe/MgO/Fe MTJ. It is found that the TMR in the SB-MTJ is 122%, while that in the DB-MTJ is 802%, increased nearly by one order of magnitude.

To substantiate the main idea of this work, we constructed a SB-MTJ and a DB-MTJ with MgO(100) as the tunnel barrier and Fe(100) as the magnetic leads, as shown in Figs. 1(a) and 1(b). Each tunnel barrier consists of three MgO atomic layers. The atomic plane terminations at each Fe/MgO interface are chosen such that the O atoms in the MgO plane are directly located above the Fe atoms, which results in the most stable structure due to the strongest Coulomb attractive interaction between the Fe cations and O anions in contact. Both the SB-MTJ and the DB-MTJ have a symmetric structure with respect to the central vertical plane; in this way the transmission probability through the two barriers in the DB-MTJ will be the same. The central Fe region with 15 Fe atomic planes is much longer than each MgO barrier to mimic a third lead connecting the two barriers.

The structural relaxation and electronic structure calculations are performed by density functional theory as implemented in the Vienna *Ab initio* Simulation Package (VASP),[36] while the transport studies are performed by the Nanodcal package.[37,38] The initial lattice constant (4.054 Å) of $\sqrt{2} \times \sqrt{2}$ Fe(100) in the transverse direction is very close to that (4.21 Å) of 1×1 Mg(100), which leads to a lattice mismatch of $\sim 3.78\%$. In the structural relaxation, following the routine in the literature,[39–41] the *xy* plane lattice constant is fixed to that of the Fe(100) substrate, while the atomic coordinates and *z*-direction lattice constant are fully optimized. The structure relaxation performed by VASP takes an energy cutoff of 600 eV and is deemed to be converged when each force component on each atom gets smaller than 0.01 eV/Å. The Perdew–Burke–Ernzerhof (PBE) form of exchange-correlation potential under generalized gradient approximation (GGA)[42] is adopted. The basis set for transport calculations are chosen as the DZP type. The energy tolerance of the electronic structure calculations of either the lead or the central region is chosen as 0.0001. The *k*-point sampling grid is chosen as $9 \times 9 \times 1$ for the self-consistency calculation and $30 \times 30 \times 1$ for the transmission function calculations.

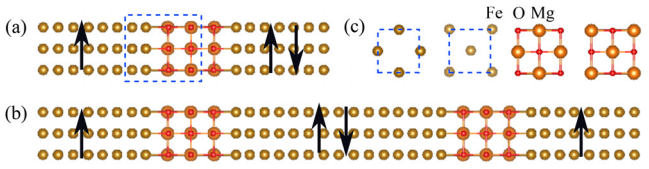

FIG. 1. The geometry structure of the magnetic tunnel junction: (a) Fe(100)/MgO (100)/Fe(100) SB-MTJ; (b) Fe(100)/MgO(100)/Fe(100)/MgO(100)/Fe(100) DB-MTJ. (c) The four sequential atomic planes around the Fe(100)/MgO(100) interface as indicated in the dashed line box in (a). The arrows show the possible magnetization directions. The antiparallel magnetic configuration is achieved by reverting the magnetization in the right lead for SB-MTJ and that in the central Fe region for the DB-MTJ.

The equilibrium conductance is calculated by[30,43]

$$G = \frac{2e^2}{h} \sum_{k_\parallel} T(E_F, k_\parallel), \tag{1}$$

with e being the electron charge, h the Planck constant, and $T(E_F, k_\parallel)$ the transmission coefficient at the Fermi energy E_F and transverse Bloch wave vector $k_\parallel = (k_x, k_y)$. The tunnel magnetoresistance ratio is calculated by

$$TMR = \left| \frac{G_A - G_{AP}}{G_{AP}} \right| \times 100\% \tag{2}$$

to characterize the conductance difference between the P and AP magnetization states.

We first introduce the theoretical basis. A cartoon model for the SB-MTJ and DB-MTJ is shown in Figs. 2(a) and 2(b), respectively. In the DB-MTJ, the two barriers are connected by a magnetic metal with the same materials as the two leads. The parallel (P) and anti-parallel (AP) magnetization configurations in the SB-MTJ is realized by fixing the magnetization in the left lead while reverting the magnetization in the right lead. In contrast, in the DB-MTJ, the P and AP magnetization configurations are realized by fixing the magnetization of the two leads and reverting that of the central metal. Thus, in the AP configuration of the DB-MTJ, the electrons will experience the magnetization misalignment twice. Generally, the transmission probability (T_1) in the P configuration will be larger than that (T_2) in the AP configuration (exception may arise). The transmission function T is actually how much probability of an electron will be transmitted from the left side to the right side of the barrier. For example, $T_1 = 0.1$ means the electrons have the chance of 10% to tunnel through the barrier. For the DB-MTJ containing two identical single barriers, the electrons will tunnel through the barriers twice with equal transmission probability. As a *crude* estimation, we may think that after passing the first barrier, 90% electrons are scattered back and only 10% electrons are left. After passing the second barrier, we will have $T_1' = T_1 T_1 = 10\% \times 10\% = 1\%$ electrons arriving at the right lead. Following this logic, if we suppose $T_1 = 0.1$ and $T_2 = 0.01$, then we will have the ON/OFF ratio $n = \frac{T_1}{T_2} = 10$ for the SB-MTJ and $n' = \frac{T_1'}{T_2'} = n^2 = 100$. Thus, it will increase exponentially with n. Since $T_1 > T_2$, we will always have $n' > n$, and the TMR ratio of the DB-

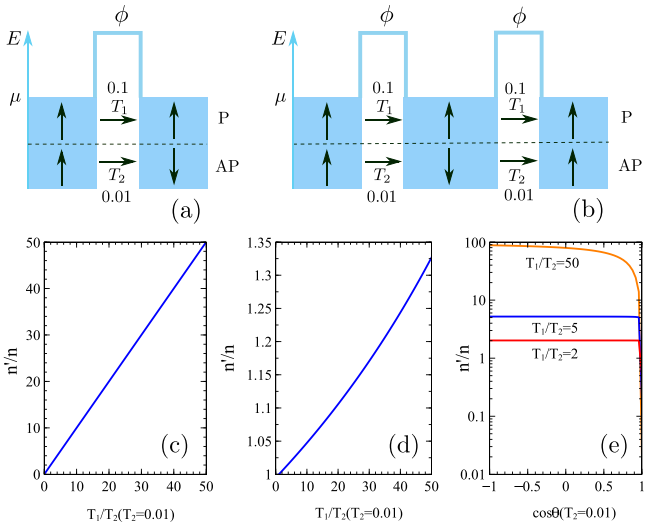

FIG. 2. A cartoon model of a MTJ with (a) single barrier; (b) double barrier, with φ indicating the tunnel barrier and μ the chemical potential of the metal, and the relationship (n'/n) between the ON/OFF ratio $(n' = T_1'/T_2')$ of the DB-MTJs and that, $n = (T_1/T_2)$, of the SB-MTJs when the DB-MTJ works in a regime of (c) an ideal independent sequential tunneling; (d) incoherent tunneling; and (e) coherent tunneling. Since it is just for a trend prediction, we assume $T_1 = 0.01$ and see how n'/n changes with $n = T_1/T_2$.

MTJ will be increased compared to that of the SB-MTJ. Since we treat the two tunneling processes through the two barriers as sequential and independent, we may call this the sequential independent tunneling [see Fig. 2(c)]. The following analysis will be more strict.

According to the quantum transport theory, in the incoherent resonant tunneling regime, for a DB structure with two identical barriers, we have $T_1' = T_1^2/(1 - R_1^2)$ and $T_2' = T_2^2/(1 - R_2^2)$,[30] where R_1 and R_2 represent the reflection probabilities corresponding to the two transmission probabilities T_1 and T_2 of the SB-MTJ under the A and AP configurations. Without loss of generality, by taking a specific $T_2 = 0.01$, we numerically consider the ON/OFF ratio $n' = \frac{T_1'}{T_2'}$ of the DB-MTJ as a function of the ON/OFF ratio $n = \frac{T_1}{T_2}$ of the SB-MTJ. It is seen that n' of the DB-MTJ is still always larger than n of the SB-MTJ [see Fig. 2(d)]. If we further take the phase shift θ between the two scatterers into account, namely, in the coherent resonant tunneling, we will have $T_1' = T_1^2/(1 - 2R_1\cos\theta + R_1^2)$, $T_2' = T_2^2/(1 - 2R_2\cos\theta + R_2^2)$.[30] It is seen that in a very wide range of $\cos\theta$, T_1'/T_2' is much larger than T_1/T_2 and only when $\cos\theta$ is very close to 1 will the ON/OFF ratio be close to 1 [see Fig. 2(e)], which means that the ON/OFF ratio will be greatly increased in most cases by changing from SB to DB in the design of the MTJs. Thus, no matter whether the DB-MTJ is in coherent tunneling regime or incoherent tunneling regime, the double barrier structure may lead to the great increase in the TMR ratio in comparison with the SB-MTJs. These preliminary estimations suggest a proposal for achieving enhanced TMR by designing DB-MTJs, which have two identical tunnel barriers in series between the two electrodes. A practical device will work at a certain point between the incoherent and coherent regime, and the actual TMR increase ratio depends on the specific system.

Figure 1 shows the relaxed structures of the Fe/MgO based SB-MTJ and DB-MTJ as proposed previously. Before moving to the transport calculations, we have first investigated the electronic structures of the Fe lead and the tunnel barrier MgO materials. Their band structure and density of states (DOS) are shown in Fig. 3. Since Fe is ferromagnetic, the electronic band structure and density of states show the obvious spin polarization feature [see Figs. 3(a) and 3(b)]. MgO is an insulator, with a wide bandgap of 5.0 eV [see Fig. 3(c)]. Since the electron transmission will decay exponentially with the insulator thickness, in this work, only three atomic MgO layers will be chosen for each tunnel barrier.

At first, we have studied the transport properties of the SB-MTJ, with the electron transmission function presented in Fig. 4(a). "U" for "up" and "D" for "down" mean the magnetization directions of the leads. Thus, "UU" means a P configuration with the magnetization directions in both leads pointing up, while "UD" means an AP configuration with magnetization up in the left lead and magnetization down in the right lead. It is seen that the electron transmission in the P configuration is much larger than that in the AP configuration. The UU curve is obviously higher than the UD curve. Specifically, at the Fermi level, for the UU configuration, $T_\uparrow = 2.344 \times 10^{-2}$, $T_\downarrow = 1.261 \times 10^{-2}$. For the "UD" configuration, $T_\uparrow = 4.214 \times 10^{-3}$, $T_\downarrow = 1.201 \times 10^{-2}$. This will give rise to an ON/OFF ratio of 2.22, which corresponds to a TMR ratio of 122%. This value is a little larger than the experimentally reported one (88%),[44] most probably because the tunnel barrier in this work is thinner than that in the literature. In the following, for simplicity, we will not discuss the TMR ratio, but the ON/OFF ratio instead. Another feature is that in the UU configuration, the transmission curve is much smoother than that in the UD configuration.

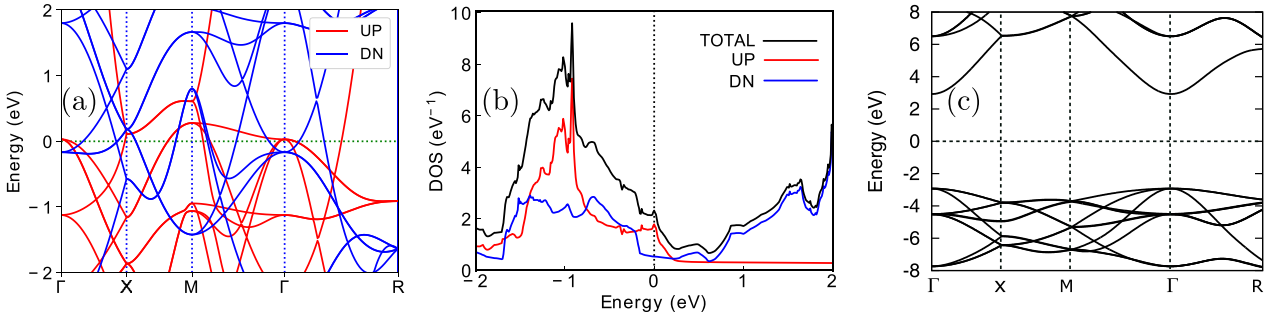

FIG. 3. (a) The band structure and (b) the density of states (DOS) of Fe(100) calculated with a rectangular supercell of 4.054 × 4.054 × 2.866 Å; and (c) the band structure of MgO(100) calculated with a cubic supercell of 4.054 × 4.054 × 4.054 Å. "UP" and "DN" means spin up and spin down, respectively.

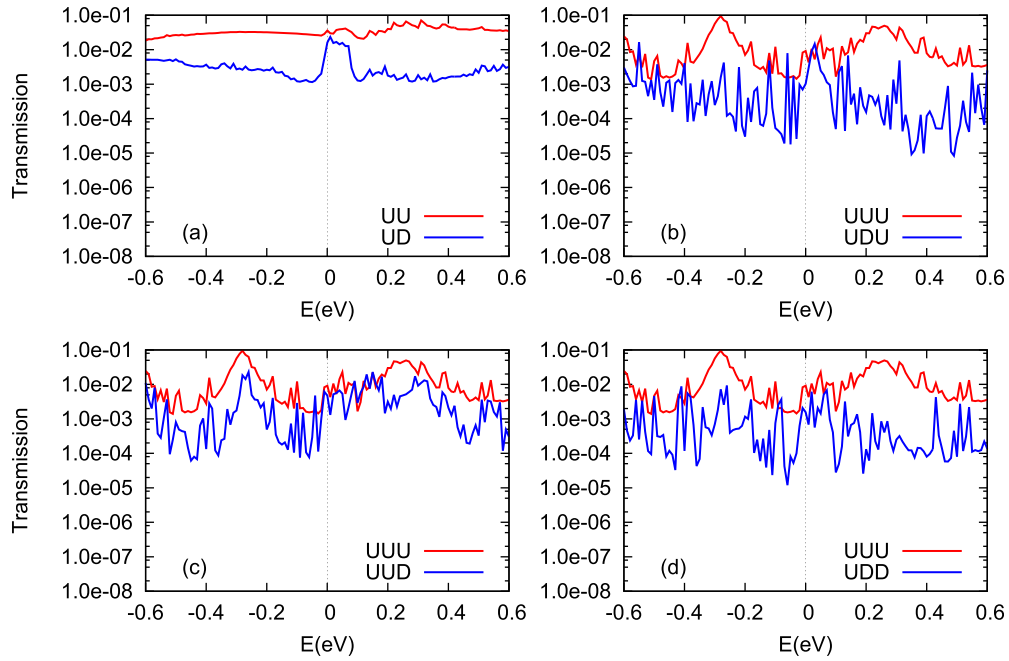

FIG. 4. The total transmission function ($T_{\uparrow} + T_{\downarrow}$) under different magnetization configurations for (a) SB-MTJ and DB-MTJ for (b) UUU and UDU; (c) UUU and UUD; and (d) UUU and UDD. "U" means magnetization pointing up, while "D" means magnetization pointing down.

To get a deeper insight of the transmission, we have performed the k-resolved transmission analysis at the Fermi level, and it is shown in Fig. 5. For the UU configuration, the main contributing channels in the spin up channel are centered around the Γ point, and the most conducting k is located at a circle at some distance to the Γ point [see Fig. 5(a)]. In contrast, the spin down channel demonstrates completely different features. The most conducting states are not around the Γ point, but evenly distributed around the diagonal lines of the $k_x - k_y$ coordinate system, with a C_4 symmetry [see Fig. 5(c)]. For the UD anti-parallel magnetic configuration, C_4 symmetry is also observed,

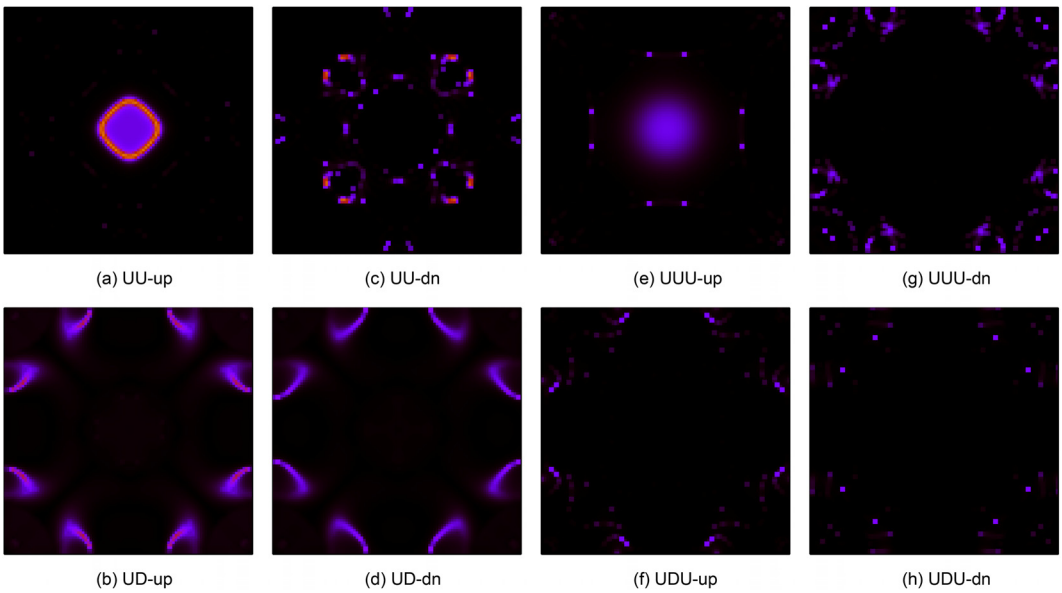

FIG. 5. The k-resolved transmission for (a)–(d) the single barrier MTJ under UU and UD configurations, respectively, and (e)–(h) for double barrier MTJ under UUU and UDU configurations, respectively, where "up" means spin up channel and "dn" means spin down channel. Yellow indicates the maximum and black indicates the minimum.

but with a different pattern and much decreased transmission [see Figs. 5(b) and 5(d)]. By comparing Fig. 5(a) and 5(c) or Figs. 5(b) and 5(d), it is seen that, after the magnetization reversal, the contributing k points are changed. Especially, the contribution of the k points around the Γ points in the spin up channel under UU configuration becomes negligible under UD configuration when the magnetization direction is reversed due to spin mismatch [Fig. 5(b)]. On the other hand, eight hot spots appear where electron transmission is considerable due to spin matching. The case is similar in the spin down channel [Figs. 5(d)].

In the DB-MTJ [see Fig. 4(b)], under the UUU parallel configuration, the spin up transmission curve is not as smooth as that in the SB-MTJ due to the sequential tunneling twice. In the UDU anti-parallel configuration, the oscillation becomes much sharper in the transmission curve, but the overall trend follows exactly the same as that of the UUU configuration, so that the UDU curve is much lower than that of UUU. Specifically, at the Fermi level, for the UUU configuration, $T_{\uparrow} = 1.70 \times 10^{-3}$, $T_{\downarrow} = 7.51 \times 10^{-3}$. For the UDU configuration, $T_{\uparrow} = 9.81 \times 10^{-4}$, $T_{\downarrow} = 3.94 \times 10^{-5}$. This will give rise to an ON/OFF ratio of 9.02 or a TMR ratio of 802%, which is greatly increased as compared to the ON/OFF ratio of 2.22 in the SB-MTJ. The $k-$ resolved transmission in the UUU and UDU states show similar features as the UU and UD in the SB-MTJs [see Figs. 5(e)–5(h)].

As a matter of fact, the functions of the DB-MTJ can be further expanded based on the fact that the magnetization directions of the three magnetic leads can be controlled separately. When the magnetization of the left lead is fixed and those of the central and right leads are flexible to flip, we will have UUU, UUD, UDU, and UDD magnetic configurations. The calculations indicate that for the UUD configuration, the equilibrium transmission, $T_{\uparrow} = 1.28 \times 10^{-4}$, $T_{\downarrow} = 4.58 \times 10^{-3}$. For the UDD configuration, $T_{\uparrow} = 1.53 \times 10^{-3}$, $T_{\downarrow} = 2.55 \times 10^{-5}$. Thus, all the four configurations have different conductances, and the DB-MTJ may achieve multiple resistance states, very promising as multi-state memory devices. Specifically, if we take the UUU state with the largest conductance as the ON state and others as OFF states, then the ON/OFF ratio of these two states are 1.95 (UUD) and 5.91 (UDD), respectively. Another important parameter characterizing the performance of an electronic device is the resistance-area product (RA), which should be as small as possible. Based on the transmission function and the cross-sectional area, the RA for the UUU, UDD, UUD, and UDU is obtained as 0.231, 0.452, 1.366, and 2.086 $\Omega \cdot \mu m^2$, respectively. Practically, due to the second barrier, the resistance of the device will be increased as compared with the single barrier case, which may slow down the operation speed. However, this can be improved by using thinner barrier layers. The extremely low RA product as obtained earlier indicates that large current density can still be produced if the barriers are thin enough.

Finally, we briefly discuss the electrical operation of the DB-MTJs. Currently, the main electrical operation schemes are the spin transfer torque (STT) and spin–orbit torque (SOT). Due to the added complexity and resistance in the double barrier design, an appropriate electrical operation scheme is needed. If the central magnetic region is taken as the free magnetic layer, the SOT mechanism may not be applicable, but the STT mechanism can still be valid. For certain systems in which a greatly increased ON/OFF ratio can be achieved by reverting the magnetization of the other substrate, both SOT and STT will work, and further, the SOT mechanism will suffer much less from the increased resistance because of the second barrier since the writing current does not pass by the tunnel barrier, while the reading can be finished by a small current.

In conclusion, we have designed a type of MTJ with double barriers and expected that the TMR ratio would be enhanced. By taking the traditional MTJ as an example, which is constructed with MgO (100) as the barrier and Fe(100) as the magnetic leads, we studied the ON/OFF ratio of SB-MTJ and DB-MTJ. It is found that the DB-MTJ shows greatly enhanced ON/OFF ratio. Compared with the UUU, which has the largest conductance, the ON/OFF ratio of UUD, UDD, and UDU is 1.95, 5.91, and 9.02. Especially, the ON/OFF ratio is greatly increased to 9.02 in UUU/UDU, as compared to that (2.22) of the SB-MTJ. More interestingly, since either the central magnetic lead and the right magnetic lead both have two magnetization configurations, we will achieve four resistance states, with different conductances and RA, which is important for multi-state memory applications. It is believed that the DB-MTJ will have better performance than the SB-MTJ in terms of ON/OFF ratio and may be considered in the design of MTJs as memory devices.

We acknowledge the support from the National Natural Science Foundation of China (Grant Nos. 12074230, 12474047, and 11974355), the Fund for Shanxi "1331 Project," and Research Project Supported by Shanxi Scholarship Council of China. We also acknowledge HZWTECH for providing computation facilities.

AUTHOR DECLARATIONS

Conflict of Interest

The authors have no conflicts to disclose.

Author Contributions

Xiaohong Zheng: Conceptualization (lead); Formal analysis (equal); Funding acquisition (equal); Writing – original draft (equal); Writing – review & editing (equal). **Shili Yang:** Data curation (equal); Visualization (equal). **Zhifan Zheng:** Data curation (equal); Formal analysis (equal). **Chun-Sheng Liu:** Data curation (equal); Formal analysis (equal); Writing – review & editing (equal). **Weiyang Wang:** Formal analysis (equal); Investigation (equal); Resources (equal); Writing – review & editing (equal). **Lei Zhang:** Data curation (equal); Formal analysis (equal); Investigation (equal).

DATA AVAILABILITY

The data that support the findings of this study are available from the corresponding authors upon reasonable request.

REFERENCES

[1]M. N. Baibich, J. M. Broto, A. Fert, F. N. Van Dau, F. Petroff, P. Etienne, G. Creuzet, A. Friederich, and J. Chazelas, "Giant magnetoresistance of (001)Fe/(001)Cr magnetic superlattices," Phys. Rev. Lett. **61**, 2472–2475 (1988).
[2]G. Binasch, P. Grünberg, F. Saurenbach, and W. Zinn, "Enhanced magnetoresistance in layered magnetic structures with antiferromagnetic interlayer exchange," Phys. Rev. B **39**, 4828–4830 (1989).
[3]I. Zutic, J. Fabian, and S. Das Sarma, "Spintronics: Fundamentals and applications," Rev. Mod. Phys. **76**, 323–410 (2004).
[4]F. Pulizzi, "Spintronics," Nat. Mater. **11**, 367–367 (2012).
[5]A. Hirohata, K. Yamada, Y. Nakatani, I.-L. Prejbeanu, B. Diény, P. Pirro, and B. Hillebrands, "Review on spintronics: Principles and device applications," J. Magn. Magn. Mater. **509**, 166711 (2020).

[6]Y. Qiu, C.-S. Liu, X. Shi, X. Zheng, and L. Zhang, "Momentum matching induced giant magnetoresistance in two-dimensional magnetic tunnel junctions," Phys. Chem. Chem. Phys. **25**, 25344–25352 (2023).
[7]J.-J. He, F.-W. Guo, H.-M. Ni, J.-B. Dong, W.-D. Cui, T.-Y. Lu, J.-R. Yuan, Y.-D. Guo, and X.-H. Yan, "Modulation of edge defects on dual-spin filtering in zigzag β-SiC_7 nanoribbons," J. Chem. Phys. **158**, 204105 (2023).
[8]J.-J. He, J.-B. Dong, Y. Zhang, Q.-Y. Cao, L.-X. Liu, J.-Y. Gu, M. Hua, J.-R. Yuan, and X.-H. Yan, "P_3S nanoribbons with bi-directional superior spin thermoelectric properties," Physica E **165**, 116116 (2025).
[9]R. Jiao, Q. Wei, L. Zhang, Y. Xie, J. He, Y. Zhou, L. Shen, and J. Yuan, "Enhancement and modulation of valley polarization in Janus CrSSe with internal and external electric fields," Phys. Chem. Chem. Phys. **26**, 13087–13093 (2024).
[10]J. Puebla, J. Kim, K. Kondou, and Y. Otani, "Spintronic devices for energy-efficient data storage and energy harvesting," Commun. Mater. **1**, 24 (2020).
[11]P. Barla, V. K. Joshi, and S. Bhat, "Spintronic devices: A promising alternative to CMOS devices," J. Comput. Electron. **20**, 805–837 (2021).
[12]B. Chen, M. Zeng, K. H. Khoo, D. Das, X. Fong, S. Fukami, S. Li, W. Zhao, S. S. Parkin, S. Piramanayagam, and S. T. Lim, "Spintronic devices for high-density memory and neuromorphic computing—A review," Mater. Today **70**, 193–217 (2023).
[13]S. M. Yakout, "Spintronics: Future technology for new data storage and communication devices," J. Supercond. Novel Magn. **33**, 2557–2580 (2020).
[14]M. G. Reuter, "A unified perspective of complex band structure: Interpretations, formulations, and applications," J. Phys.: Condens. Matter **29**, 053001 (2017).
[15]N. F. Hinsche, M. Fechner, P. Bose, S. Ostanin, J. Henk, I. Mertig, and P. Zahn, "Strong influence of complex band structure on tunneling electroresistance: A combined model and ab initio study," Phys. Rev. B **82**, 214110 (2010).
[16]A. Jensen, M. Strange, S. Smidstrup, K. Stokbro, G. C. Solomon, and M. G. Reuter, "Complex band structure and electronic transmission eigenchannels," J. Chem. Phys. **147**, 224104 (2017).
[17]E. Y. Tsymbal, O. N. Mryasov, and P. R. LeClair, "Spin-dependent tunnelling in magnetic tunnel junctions," J. Phys.: Condens. Matter **15**, R109–R142 (2003).
[18]J.-G. J. Zhu and C. Park, "Magnetic tunnel junctions," Mater. Today **9**, 36–45 (2006).
[19]L. Zhang, J. Zhou, H. Li, L. Shen, and Y. P. Feng, "Recent progress and challenges in magnetic tunnel junctions with 2D materials for spintronic applications," Appl. Phys. Rev. **8**, 021308 (2021).
[20]P. Dey and J. N. Roy, "Tunnelling magnetoresistance (TMR)," in *Spintronics: Fundamentals and Applications* (Springer, Singapore, 2021), pp. 103–125.
[21]H. Jin and T. Miyazaki, "Tunnel magnetoresistance effect," in *The Physics of Ferromagnetism* (Springer Berlin Heidelberg, Berlin, Heidelberg, 2012), pp. 403–432.
[22]J.-Y. Chen, Y.-C. Lau, J. M. D. Coey, M. Li, and J.-P. Wang, "High performance MgO-barrier magnetic tunnel junctions for flexible and wearable spintronic applications," Sci. Rep. **7**, 42001 (2017).
[23]X. Liu and J. Shi, "Magnetic tunnel junctions with Al_2O_3 tunnel barriers prepared by atomic layer deposition," Appl. Phys. Lett. **102**, 202401 (2013).
[24]T. Miyazaki and N. Tezuka, "Giant magnetic tunneling effect in Fe/Al_2O_3/Fe junction," J. Magn. Magn. Mater. **139**, L231–L234 (1995).
[25]S. Yuasa, T. Nagahama, A. Fukushima, Y. Suzuki, and K. Ando, "Giant room-temperature magnetoresistance in single-crystal Fe/MgO/Fe magnetic tunnel junctions," Nat. Mater. **3**, 868–871 (2004).
[26]S. Yuasa, A. Fukushima, H. Kubota, Y. Suzuki, and K. Ando, "Giant tunneling magnetoresistance up to 410 temperature in fully epitaxial Co/MgO/Co magnetic tunnel junctions with bcc Co(001) electrodes," Appl. Phys. Lett. **89**, 042505 (2006).
[27]S. Ikeda, J. Hayakawa, Y. Ashizawa, Y. M. Lee, K. Miura, H. Hasegawa, M. Tsunoda, F. Matsukura, and H. Ohno, "Tunnel magnetoresistance of 604% at 300 K by suppression of Ta diffusion in CoFeB/MgO/CoFeB pseudo-spin-valves annealed at high temperature," Appl. Phys. Lett. **93**, 082508 (2008).
[28]M. K. Yadav and S. K. Gupta, "FeAl/MgO/FeAl MTJ with enhanced TMR and low resistance area product for MRAM: A first principle study," Micro Nanostruct. **165**, 207192 (2022).
[29]L. L. Chang, L. Esaki, and R. Tsu, "Resonant tunneling in semiconductor double barriers," Appl. Phys. Lett. **24**, 593–595 (1974).
[30]S. Datta, *Electronic Transport in Mesoscopic Systems* (Cambridge University Press, Cambridge, England, 1995).
[31]W. Xiao, X. Zheng, H. Hao, L. Kang, L. Zhang, and Z. Zeng, "Greatly enhanced tunneling electroresistance in ferroelectric tunnel junctions with a double barrier design," npj Comput. Mater. **9**, 144 (2023).
[32]N. Ghobadi and R. Daqiq, "Tunnel-magneto resistance of double-barrier tunnel junctions in the presence of spin-orbit coupling within spin-filter barriers," Physica B **673**, 415464 (2024).
[33]R. Daqiq, "Spin-filtering effects of double-barrier magnetic tunnel junctions with an indium phosphide (InP) spacer," Mater. Sci. Eng., B **263**, 114818 (2021).
[34]Z. Zeng, H. Wei, L. Jiang, G. Du, W. Zhan, and X. Han, "High magnetoresistance in Co–Fe–B-based double barrier magnetic tunnel junction," J. Magn. Magn. Mater. **303**, e219–e222 (2006).
[35]B. Li, C. Zeng, J. Zhao, J. Yang, J. G. Hou, and Q. Zhu, "Single-electron tunneling spectroscopy of single C_{60} in double-barrier tunnel junction," J. Chem. Phys. **124**, 064709 (2006).
[36]G. Kresse and J. Furthmüller, "Efficient iterative schemes for ab initio total-energy calculations using a plane-wave basis set," Phys. Rev. B **54**, 11169–11186 (1996).
[37]J. Taylor, H. Guo, and J. Wang, "*Ab initio* modeling of quantum transport properties of molecular electronic devices," Phys. Rev. B **63**, 245407 (2001).
[38]J. Maassen, M. Harb, V. Michaud-Rioux, Y. Zhu, and H. Guo, "Quantum transport modeling from first principles," Proc. IEEE **101**, 518–530 (2013).
[39]J. D. Burton and E. Y. Tsymbal, "Giant tunneling electroresistance effect driven by an electrically controlled spin valve at a complex oxide interface," Phys. Rev. Lett. **106**, 157203 (2011).
[40]Y. W. Yin, J. D. Burton, Y.-M. Kim, A. Y. Borisevich, S. J. Pennycook, S. M. Yang, T. W. Noh, A. Gruverman, X. G. Li, E. Y. Tsymbal, and Q. Li, "Enhanced tunnelling electroresistance effect due to a ferroelectrically induced phase transition at a magnetic complex oxide interface," Nat. Mater. **12**, 397–402 (2013).
[41]L. N. Jiang, W. Z. Chen, B. S. Yang, X.-G. Zhang, Y.-P. Wang, and X. F. Han, "First-principles prediction of switchable metallic ferroelectricity in multiferroic tunnel junctions," Phys. Rev. B **99**, 224103 (2019).
[42]J. P. Perdew, K. Burke, and M. Ernzerhof, "Generalized gradient approximation made simple," Phys. Rev. Lett. **77**, 3865–3868 (1996).
[43]H. Haug and A.-P. Jauho, *Quantum Kinetics in Transport and Optics of Semiconductors* (Springer-Verlag, Berlin, 1996).
[44]T. Nozaki, A. Hirohata, N. Tezuka, S. Sugimoto, and K. Inomata, "Bias voltage effect on tunnel magnetoresistance in fully epitaxial MgO double-barrier magnetic tunnel junctions," Appl. Phys. Lett. **86**, 082501 (2005).